arXiv:1406.4762v1 [cond-mat.mes-hall] 18 Jun 2014

Projective versus weak measurement of charge in a mesoscopic conductor

D. Oehri,[1] A.V. Lebedev,[1] G.B. Lesovik,[2] and G. Blatter[1]

[1] *Theoretische Physik, ETH Zurich, CH-8093 Zurich, Switzerland*
[2] *L.D. Landau Institute for Theoretical Physics RAS, 117940 Moscow, Russia*

(Dated: June 19, 2014)

We study the charge dynamics of a quantum dot as measured by a nearby quantum point contact probing the dot via individual single-particle wave packets. We contrast the two limiting cases of weak and strong system–detector coupling exerting vanishing and strong back-action on the system and analyze the resulting differences in the charge-charge correlator. Extending the study to multiple projective measurements modelling a continuous strong measurement, we identify a transition from a charge dynamics dominated by the system's properties to a universal dynamics governed by the measurement.

PACS numbers: 73.23.-b 03.65.Ta

I. INTRODUCTION

Discussions on quantum measurement[1–3] usually rely on two fundamental elements, the Born rule[4], telling us how to extract information from the quantum mechanical wave function, and the von Neumann[5] projection postulate, stating that measuring a system observable generates a collapse of the wave function and telling us how to restart the system's unitary evolution after the measurement. A third most important element is that of the detector's back-action on the system which is at the heart of the projection process when viewed from a microscopic perspective; much effort has gone into the understanding of the phenomenological von Neumann projection in terms of a unitary evolution of the entangled system–detector dynamics. Here, we take a step back and study the charge dynamics, specifically the charge-charge correlator, of a quantum dot (QD) as measured by a quantum point contact (QPC) in order to understand the impact of the detector's back-action on the time evolution of the correlator. We study the impact of the back-action in two limiting cases: i) a weak detector–system coupling which we treat perturbatively describing the limit of no back-action and ii) an intermediate/strong system–detector coupling which we describe by a von Neumann projection accounting for the limit of strong back-action. We determine the physically measureable correlators and quantitatively analyze their difference for the case of a quantum dot with a single resonant level.

Understanding quantum measurement as the bridge between the quantum- and our classical work is a fascinating and broad topic, ranging from fundamental aspects of the measurement problem[6–9] to such practical issues as optimizing the information gain at minimal system invasion[10]. Much effort has gone into the microscopic understanding of the measurement process and its interrelation with back-action, treating quantum averaged evolutions[11–16], selective system dynamics[17,18], and correlated weak-strong measurements in the form of weak values[19–22]. Quantum dots in transport[11,12,22–24], isolated double quantum dots[15–18,21], as well as quantum point contacts[25–28] have played a central role in analyzing quantum measurement within the realm of mesoscopic physics.

In the present study, we focus on the charge dynamics of a quantum dot (or a localized region of a mesoscopic scatterer in more general terms) as measured by a nearby QPC detector and determine the time evolution of the average charge and the charge-charge correlator for different strengths of the system–detector coupling. Thereby we keep in mind a measurement with single-particle wave packets[29,30] incident on the detector at times t_1 and t_2 with their reflection/transmission through the QPC providing information on the charge state of the quantum dot at the two time instances. Our analysis provides us with two central results: on a technical level, we find that the strong projective measurement can be expressed through a projected charge $\hat{Q}^P(t|t_0)$, the charge at time t after a previous projection at time t_0, for which we find a compact expression in terms of the system's scattering matrix. On a physical level, we find that, in spite of the strongly different back-action induced by the first measurement, the two correlators for weak and strong measurements come out qualitatively similar, although quantitative differences remain, of course; the latter are specifically discussed for the single-resonance level model. Furthermore, we attempt to model the case of a finite constant voltage V applied to the QPC detector by considering a sequence of wave packets incident on the QPC, leading to repeated projections which we describe via the projection postulate. Increasing the rate of projections, we identify a transition from a regime where the dynamics of the system is dominated by the system's characteristics to a regime where the dynamics is universal and uniquely determined by the measurement.

The paper is organized as follows: In Sec. II we introduce the model describing our mesoscopic conductor and discuss the different regimes of projective (intermediate/strong coupling) and weak measurements, identifying the measurable charge-charge correlator in each of these regimes. In Sec. III, the two charge-charge correlators are calculated for arbitrary scatterers and their difference is discussed quantitatively for the case of a single-level quantum dot. In Sec. IV, the discussion is extended

to the case of repeated projective measurements. In order to understand the universal behavior found for fast repeated measurements, we consider the model of a fluctuating quantum dot level. A summary and conclusions are given in Sec. V.

II. FORMALISM

We consider a mesoscopic conductor with a central scattering region (e.g., a quantum dot), described through its single-particle scattering matrix $\mathbf{S}_k$ (see Ref. 31 for a review on the scattering matrix approach to mesoscopic transport). Here, we are interested in the dynamics of the charge $Q(t)$ (measured in units of electronic charge e) in the scattering region and its modifications when it is subjected to a (strong) measurement. In order to measure this dynamics and specifically the associated charge-charge correlator, the scattering region is capacitively coupled to the quantum point contact (QPC) of a detector system, see Fig. 1. The charge dynamics $Q(t)$ of the system and the current $I_{\mathcal{M}}(t)$ through the detector then mutually influence one another and we have to analyze the measurement process in order to identify the measurable charge-charge correlator.

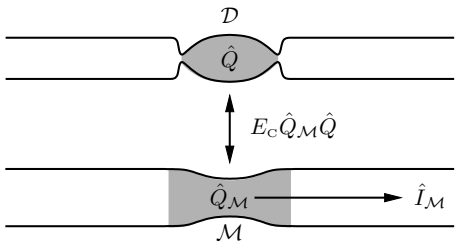

FIG. 1: The system of interest with the central region $\mathcal{D}$ holding the charge $\hat{Q}$ (here a quantum dot) capacitively coupled to the central region $\mathcal{M}$ of the measurement system. The current $\hat{I}_{\mathcal{M}}$ in the detector serves as a readout for the charge $\hat{Q}$ in the region $\mathcal{D}$.

A. The model system

We consider a one-dimensional non-interacting system consisting of two half-infinite leads connected through a central region $\mathcal{D} = [-d/2, d/2]$ where particles are scattered by the single-particle potential $\hat{V}$. The latter is characterized by the single-particle scattering matrix

$$\mathbf{S}_k = \begin{pmatrix} r_{Lk} & t_k \\ t_k & r_{Rk} \end{pmatrix}. \tag{1}$$

We make use of the Lippmann-Schwinger scattering states $|\varphi_{ak}\rangle$ satisfying $(\hat{H}_{\rm kin} + \hat{V})\,|\varphi_{ak}\rangle = \epsilon_k\,|\varphi_{ak}\rangle$ with the kinetic part of the Hamiltonian $\hat{H}_{\rm kin}$, the wavevector $k > 0$ and $a = L/R$ describing a scattering state incoming from the left/right. We linearize the spectrum around the Fermi energy $\epsilon_{\rm F}$, i.e., $\epsilon_k = \epsilon_{\rm F} + \hbar v_{\rm F}(k - k_{\rm F})$. The asymptotics $|x| \to \infty$ of the (LS) scattering states is described by the scattering amplitudes, i.e.,

$$\begin{aligned} \varphi_{Lk} &\sim \Theta(-x)(e^{ikx} + r_{Lk}e^{-ikx}) + \Theta(x)t_k e^{ikx}, \\ \varphi_{Rk} &\sim \Theta(-x)t_k e^{-ikx} + \Theta(x)(e^{-ikx} + r_{Rk}e^{ikx}). \end{aligned} \tag{2}$$

Spin is trivially accounted for in our non-interacting system and hence we restrict ourselves to spinless particles.

As shown in Refs. 27 and 32, the operator $\hat{Q}$ describing the charge in the central region $\mathcal{D}$ (in units of the electronic charge e) can be expressed through creation (annihilation) operators $\hat{c}^\dagger_{ak}$ ($\hat{c}_{ak}$) of the above Lippmann-Schwinger scattering states via

$$\hat{Q}(t) = \sum_{a'a} \int \frac{dk'}{2\pi} \int \frac{dk}{2\pi} A_{a'k',ak}(t) \hat{c}^\dagger_{a'k'} \hat{c}_{ak} \tag{3}$$

$$= \sum_{\alpha'\alpha} A_{\alpha',\alpha}(t) \hat{c}^\dagger_{\alpha'} \hat{c}_\alpha, \tag{4}$$

with the notation $\alpha = (a, k)$ and $\sum_\alpha = \sum_a \int (dk/2\pi)$. The matrix elements $A_{\alpha',\alpha}(t) = [\mathbf{A}_{k',k}(t)]_{a',a}$ are related to the scattering matrix $\tilde{\mathbf{S}}_k = \mathbf{S}_k e^{ikd}$,

$$\mathbf{A}_{k',k}(t) = -i \frac{\mathbf{1} - \tilde{\mathbf{S}}^\dagger_{k'} \tilde{\mathbf{S}}_k}{k' - k} e^{i(k'-k)(v_{\rm F}t + d/2)} \tag{5}$$

with $\mathbf{A}_{k,k}(t) = -i\tilde{\mathbf{S}}^\dagger_k \partial_k \tilde{\mathbf{S}}_k$ and where we have dropped terms of order $\mathcal{O}(1/k_{\rm F})$. The matrix $\mathbf{A}$ is equivalent to the density of states matrix expression introduced in Ref. 33 and was used in Ref. 32 to express the interaction kernel through the scattering states in a discussion of interacting electron transport; here, it is used to express the charge through the scattering states, see Eq. (4), and to obtain simple and compact expressions for the projected charge, see Eqs. (23) and (27). With regard to the latter, we note that the matrix $\mathbf{A}$ possesses the useful projector property

$$\int \frac{dp}{2\pi} \mathbf{A}_{k,p}(t) \mathbf{A}_{p,q}(t) = \mathbf{A}_{k,q}(t), \tag{6}$$

a consequence of the projector property $\hat{Q}(t)\hat{Q}(t) = \hat{Q}(t)$ of the charge operator restricted to the single-particle Hilbert space; the latter is easily checked by acting (twice) with the charge operator $\hat{Q}(t) \equiv \hat{\mathcal{P}}_{\mathcal{D}}(t) = \int_{\mathcal{D}} dx\, \hat{\psi}^\dagger(x,t)\hat{\psi}(x,t)$ on a single-particle state $|\Psi_1\rangle$ (here, $\hat{\mathcal{P}}_{\mathcal{D}}(t)$ denotes the real-space projector on the region $\mathcal{D}$). The transport through $\mathcal{D}$ is implemented by connecting the two semi-infinite leads to two reservoirs at chemical potential μ_L and μ_R with $\mu_{L/R} = \epsilon_{\rm F} \pm eV/2$ as described by the steady state density matrix $\hat{\rho}_0$.

Within this model, we are able to describe local properties of the system, specifically the charge dynamics in the region $\mathcal{D}$, through the single-particle scattering matrix $\mathbf{S}_k$ which is an asymptotic property of the system.

Note that interactions are limited to the system–detector coupling, i.e., we are considering a non-interacting system; interactions within the system could be taken into account within perturbation theory[32].

B. The detector

In order to measure the system charge $\hat{Q}$ we make use of a capacitively coupled QPC detector[25]. The latter is characterized by a step-like transmission characteristic, see Fig. 2, with a width $h\Gamma$ related to the tunneling time $t_{\rm tun} \sim 1/\Gamma$ of particles traversing the constriction. The coupling $\hat{H}_{\rm coupl} = E_{\rm C}\hat{Q}_{\mathcal{M}}\hat{Q}$ between the system charge $\hat{Q}$ and the charge $\hat{Q}_{\mathcal{M}}$ in the QPC region $\mathcal{M}$ of the detector will shift the location of the transmission step and the detector current will provide information about the system, while at the same time cause an unavoidable back-action.

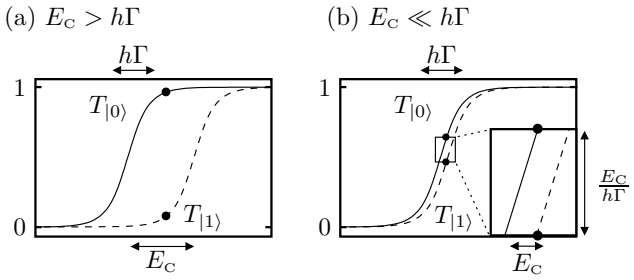

FIG. 2: (a) The QPC transmission changes from 0 to 1 within a width $h\Gamma$. In the case of strong coupling $E_{\rm C} > h\Gamma$, the change of transmission between $T_{|0\rangle}$ (empty dot) and $T_{|1\rangle}$ (filled dot) can be tuned to about unity (see black dots). (b) For weak coupling, $E_{\rm C} \ll h\Gamma$, the change of transmission (see black dots) is small, i.e., $\Delta T \approx E_{\rm C}/h\Gamma \ll 1$.

To fix ideas, we restrict the discussion to a single-level quantum dot (QD) with two charge states $|0\rangle$ and $|1\rangle$ and focus on the limit where each detector electron probes the dot individually, requiring that the tunneling time $t_{\rm tun} \sim 1/\Gamma$ is small compared to the typical separation between detector electrons (alternatively, we can consider a weakly driven detector with bias voltage $eV \ll h\Gamma$ such that the typical time separation $t_V \sim h/eV > t_{\rm tun}$ between electrons is large). In order for the detector to measure the system it should be fast, $t_{\rm tun} \ll t_{\rm sys}$, where $t_{\rm sys}$ is a typical system timescale. In this situation, the system is in a fixed charge state during the tunneling of a detector electron. If the QD is empty (state $|0\rangle$), the electron is transmitted with probability $T_{|0\rangle} \approx T(\epsilon_{\rm F})$, while for a filled QD (state $|1\rangle$), the transmission probability is $T_{|1\rangle} \approx T(\epsilon_{\rm F} - E_{\rm C})$. We then identify two measurement regimes: i) a strong coupling regime with $E_{\rm C} > h\Gamma$, see Fig. 2(a), where we can choose a working point such that $T_{|0\rangle} \approx 1$ and $T_{|1\rangle} \approx 0$, and ii) a weak coupling regime $E_{\rm C} < h\Gamma$, see Fig. 2(b), where the change in transmission $\Delta T = T_{|0\rangle} - T_{|1\rangle} \approx E_{\rm C}/h\Gamma \ll 1$ is small.

C. Projective measurement

For strong coupling, $E_{\rm C} > h\Gamma$ the charge states of the dot and the state of one single QPC electron after scattering [i.e., transmitted ($|t\rangle$) or reflected ($|r\rangle$)] become fully entangled, $\alpha|0\rangle \otimes |t\rangle + \beta|1\rangle \otimes |r\rangle$. The detection of this electron leads to the 'collapse' of the dot state and fully determines the charge, such that the measurement with even a single QPC electron is a strong one, able to acquire the full information; the concomitant projection of the dot state corresponds to the strongest possible back-action of the detector on the system. Hence, in order to measure the charge $\hat{Q}(t)$ at time t at strong coupling $E_{\rm C} > h\Gamma$, one single electron[29,30] is sent towards the QPC to arrive there at time t. The detection of the transmitted electron determines the charge state of region $\mathcal{D}$ and projects the system to the corresponding state. Repeating this measurement (after the system has equilibrated) allows to determine the average charge Q. Similarly, in order to measure the charge-charge correlator, the dot charge has to be measured at times t_1 and t_2 and the measurement has to be repeated after equilibration at fixed time delay $\Delta t = t_2 - t_1$ in order to find the average charge-charge correlator for times t_1 and t_2.

In order to describe this correlator theoretically, we describe the measurement using the projection postulate[5]: the measurement of the charge operator $\hat{Q}$ at t projects the system onto a state with an integer number of charges in the central region $\mathcal{D}$ which we account for by the operator

$$\hat{P}_N(t) = \int_0^{2\pi} \frac{d\lambda}{2\pi} e^{i\lambda(\hat{Q}(t)-N)} \tag{7}$$

projecting the state of the system at time t onto a state with N charges in the central region $\mathcal{D}$. While the system's state for times $t' < t$ is described by the steady-state density matrix $\hat{\rho}_0$, the charge measurement at time t projects the density matrix onto well-defined charge states which are expressed through the operator $\hat{P}_N$ as $\sum_N \hat{P}_N(t)\hat{\rho}_0\hat{P}_N(t)$. Then the *projected* charge-charge correlator at times t_1 and $t_2 > t_1$ is given by

$$S^P_{QQ}(t_2,t_1) = \sum_N {\rm Tr}\Big\{\hat{Q}(t_2)\hat{Q}(t_1)\hat{P}_N(t_1)\hat{\rho}_0\hat{P}_N(t_1)\Big\}, \tag{8}$$

where the collapse of the state at time t_1 is accounted for by the projection operators $\hat{P}_N(t_1)$ while the measurement at time t_2 does not affect the result. Making use of the cyclic property of the trace and $[\hat{Q}(t_1), \hat{P}_N(t_1)] = 0$, we obtain the projected correlator

$$S^P_{QQ}(t_2,t_1) = \langle \hat{Q}^P(t_2|t_1)\hat{Q}(t_1)\rangle, \tag{9}$$

with $\langle\hat{O}\rangle = {\rm Tr}\{\hat{O}\hat{\rho}_0\}$ and the operator $\hat{Q}^P(t_2|t_1)$ describing the charge in the central region at time t_2 provided

that the state of the system was projected at time $t_1 < t_2$,

$$\hat{Q}^P(t_2|t_1) = \sum_N \hat{P}_N(t_1)\hat{Q}(t_2)\hat{P}_N(t_1). \tag{10}$$

Eq. (9) corresponds to the measurable charge-charge correlator in the regime of strong, projective measurements. Taking into account the spin degree of freedom, Eq. (9) remains unchanged with $\hat{Q}(t_1) = \hat{Q}_\downarrow(t_1) + \hat{Q}_\uparrow(t_1)$ and $\hat{Q}^P(t_2|t_1) = \hat{Q}^P_\downarrow(t_2|t_1) + \hat{Q}^P_\uparrow(t_2|t_1)$; furthermore, the up- and down spin components of charge are uncorrelated.

At intermediate coupling $E_\mathrm{C} < h\Gamma$ the scattering of one single electron becomes a probabilistic process (with finite transmission and reflection probability for both charge states) such that one electron alone does not provide the information on the dot's state and many electrons are required to probe the dot. The full information about the dot state is acquired after the passage of N electrons when the measured transmitted charge $Q_\mathrm{tr}(N)$ through the QPC can be attributed to a particular dot state, i.e., the difference $Q_\mathrm{tr}^{|0\rangle}(N) - Q_\mathrm{tr}^{|1\rangle}(N) = \Delta T\, N$ has to be larger than the standard deviation σ of the probabilistic process of charge transmission. At small temperatures, the latter is determined by the charge partitioning noise, i.e., $\sigma^2 = T(1-T)\,N$, such that the required number of probe electrons is[11,12,15,16]

$$N \sim \Big(\frac{h\Gamma}{E_\mathrm{C}}\Big)^2 T(1-T). \tag{11}$$

For the case where a finite voltage V is applied across the QPC detector, we obtain the measurement time $t_\mathrm{ms} \sim N t_V$ with $t_V = h/eV$ the voltage time. For small temperatures $k_\mathrm{B}T < eV$ the partitioning noise dominates over the thermal noise.

Next, we have to account for the time scale t_sys of the dot. For $t_\mathrm{ms} \ll t_\mathrm{sys}$, the state of the dot can be determined by probing the dot for some measurement time larger than t_ms; such a measurement is strong and projective. On the other hand, the measurement is generically weak if $t_\mathrm{ms} > t_\mathrm{sys}$ and we have to find an alternative procedure to find the information on the dot's charge state; we will discuss this weak measurement regime in the next section.

The discussion in this section has been limited to the case of a single-level quantum dot, however, the extension to the case of a more complex system with more charge states is straightforward. While in such a situation it is not possible to resolve all charge states by one electron alone, a projective measurement involving many electrons or a weak measurement as described below are still possible.

D. Weak coupling, weak measurement regime

At generically weak coupling $E_\mathrm{C} \ll h\Gamma$ (such that $t_\mathrm{ms} > t_\mathrm{sys}$), the system cannot be measured during the system time t_sys and we need an alternative measurement scheme. The capacitive coupling between the system and the detector still affects the detector current $\hat{I}_\mathcal{M}$ and thus can be used to learn about the system's charge dynamics $Q(t)$. The detector current is given by the expectation value $\langle \hat{I}^H_\mathcal{M}(x,t)\rangle = \mathrm{Tr}\{\hat{I}^H_\mathcal{M}(x,t)\,\hat{\rho}_\mathrm{sd}\}$, where $\hat{I}^H_\mathcal{M}(x,t)$ is the current operator in the Heisenberg representation and $\hat{\rho}_\mathrm{sd}$ is the steady-state density matrix of the combined system–detector setup, $\hat{\rho}_\mathrm{sd} = \hat{\rho}_0 \otimes \hat{\rho}_0^\mathcal{M}$. For a weak system–detector coupling, we can calculate the modulation in the detector current perturbatively[27,34–36]; to lowest order in the coupling strength E_C the result is

$$\langle \hat{I}^H_\mathcal{M}(x,t)\rangle \approx \langle \hat{I}_\mathcal{M}(x,t)\rangle + \frac{2E_\mathrm{C}}{\hbar}\int_{-\infty}^{t} d\tau\, \mathcal{I}S^\mathcal{M}_{IQ}(x,t;\tau)\langle \hat{Q}(\tau)\rangle, \tag{12}$$

where $\hat{I}_\mathcal{M}(x,t)$ is the current operator in the interaction representation (i.e., with respect to the coupling Hamiltonian) and $\langle\hat{\mathcal{O}}\rangle = \mathrm{Tr}\{\hat{\mathcal{O}}\,\hat{\rho}_\mathrm{sd}\}$. In the expression above, $\mathcal{I}S^\mathcal{M}_{IQ}(x,t;\tau)$ is the imaginary part of the correlator between the detector current $\hat{I}_\mathcal{M}(x,t)$ and the detector charge $\hat{Q}_\mathcal{M}(\tau)$, i.e., $\mathcal{I}S^\mathcal{M}_{IQ}(x,t;\tau) = -i\langle\langle[\hat{I}_\mathcal{M}(x,t),\hat{Q}_\mathcal{M}(\tau)]\rangle\rangle/2$ with $\langle\langle\hat{\mathcal{O}}_1\hat{\mathcal{O}}_2\rangle\rangle = \langle\hat{\mathcal{O}}_1\hat{\mathcal{O}}_2\rangle - \langle\hat{\mathcal{O}}_1\rangle\langle\hat{\mathcal{O}}_2\rangle$. The quantity $\mathcal{I}S^\mathcal{M}_{IQ}(x,t;\tau)$ is a response function of the measurement apparatus $\mathcal{M}$ and hence a pure detector property, independent of the system. A good detector is much faster than the dynamics of the system of interest, i.e., $t_\mathrm{tun} \ll t_\mathrm{sys}$, such that the charge $\langle\hat{Q}(\tau)\rangle$ can be treated as slowly varying on the time scale of the detector. The response function $\mathcal{I}S^\mathcal{M}_{IQ}$ then is effectively given by the zero frequency response function, i.e., $\mathcal{I}S^\mathcal{M}_{IQ}(x,t;\tau) \approx \mathcal{I}S^\mathcal{M}_{IQ,\omega=0}\delta[\tau - (t - x/v_\mathrm{F})]$, such that

$$\langle \hat{I}^H_\mathcal{M}(x,t)\rangle \approx \langle \hat{I}_\mathcal{M}(x)\rangle + \frac{2E_\mathrm{C}}{\hbar}\mathcal{I}S^\mathcal{M}_{IQ,\omega=0}\langle\hat{Q}(t-x/v_\mathrm{F})\rangle. \tag{13}$$

This relation allows one to determine the time averaged charge expectation value $\bar{Q}$ from an experimentally measured time trace of $I_\mathcal{M}(x,t)$ by calculating the time averaged current $\bar{I}_\mathcal{M} = (1/T)\int_0^T dt\, I_\mathcal{M}(x,t)$.

Next, we derive an expression for the charge correlator at times t_1 and t_2 in the weak-coupling regime. We consider two detectors[36] $\mathcal{A}$ and $\mathcal{B}$ capacitively coupled to the system, i.e., $\hat{H}_\mathrm{coupl} = E_\mathrm{C}^\mathcal{A}\hat{Q}_\mathcal{A}\hat{Q} + E_\mathrm{C}^\mathcal{B}\hat{Q}_\mathcal{B}\hat{Q}$. The correlation between the two detectors arises due to the coupling between the two detectors via the system charge. The measurable time-domain correlator of the detector is the *irreducible* symmetrized current-current correlator[37] $\langle\langle\hat{I}^H_\mathcal{A}(x_\mathcal{A},t_\mathcal{A})\hat{I}^H_\mathcal{B}(x_\mathcal{B},t_\mathcal{B}) + \hat{I}^H_\mathcal{B}(x_\mathcal{B},t_\mathcal{B})\hat{I}^H_\mathcal{A}(x_\mathcal{A},t_\mathcal{A})\rangle\rangle/2$ (in contrast to a measurement in the frequency domain, where a non-symmetrized correlator is measured at positive frequencies[38–40]). The above symmetrized detector correlator is related to the charge-charge correlator of the dot via

$$\mathcal{R}S^{\rm irr}_{I_{\mathcal{A}}I_{\mathcal{B}}}(x_{\mathcal{A}},t_{\mathcal{A}};x_{\mathcal{B}},t_{\mathcal{B}}) = \langle\langle \hat{I}^H_{\mathcal{A}}(x_{\mathcal{A}},t_{\mathcal{A}})\hat{I}^H_{\mathcal{B}}(x_{\mathcal{B}},t_{\mathcal{B}}) + \hat{I}^H_{\mathcal{B}}(x_{\mathcal{B}},t_{\mathcal{B}})\hat{I}^H_{\mathcal{A}}(x_{\mathcal{A}},t_{\mathcal{A}})\rangle\rangle/2$$
$$\approx \frac{E^{\mathcal{A}}_{\rm C}E^{\mathcal{B}}_{\rm C}}{\hbar^2}\iint_{-\infty}^{\infty} d\tau_{\mathcal{A}}d\tau_{\mathcal{B}}\Big(\Theta(t_{\mathcal{A}}-\tau_{\mathcal{A}})\Theta(t_{\mathcal{B}}-\tau_{\mathcal{B}})\mathcal{I}S^{\mathcal{A}}_{IQ}(x_{\mathcal{A}},t_{\mathcal{A}};\tau_{\mathcal{A}})\mathcal{I}S^{\mathcal{B}}_{IQ}(x_{\mathcal{B}},t_{\mathcal{B}};\tau_{\mathcal{B}})\mathcal{R}S^{\rm irr}_{QQ}(\tau_A,\tau_B)$$
$$+\Theta(t_{\mathcal{A}}-\tau_{\mathcal{A}})\Theta(\tau_{\mathcal{A}}-\tau_{\mathcal{B}})\mathcal{I}S^{\mathcal{A}}_{IQ}(x_{\mathcal{A}},t_{\mathcal{A}};\tau_{\mathcal{A}})\mathcal{R}S^{\mathcal{B}}_{IQ}(x_{\mathcal{B}},t_{\mathcal{B}};\tau_{\mathcal{B}})\mathcal{I}S^{\rm irr}_{QQ}(\tau_{\mathcal{A}},\tau_{\mathcal{B}})$$
$$-\Theta(t_{\mathcal{B}}-\tau_{\mathcal{B}})\Theta(\tau_{\mathcal{B}}-\tau_{\mathcal{A}})\mathcal{R}S^{\mathcal{A}}_{IQ}(x_{\mathcal{A}},t_{\mathcal{A}};\tau_{\mathcal{A}})\mathcal{I}S^{\mathcal{B}}_{IQ}(x_{\mathcal{B}},t_{\mathcal{B}};\tau_{\mathcal{B}})\mathcal{I}S^{\rm irr}_{QQ}(\tau_{\mathcal{A}},\tau_{\mathcal{B}})\Big), \qquad (14)$$

as follows from a perturbative analysis in the lowest order of the couplings. In the above expression,

$$\mathcal{R}S^{\mathcal{M}}_{IQ}(x,t;\tau) = \langle\langle\{\hat{I}_{\mathcal{M}}(x,t),\hat{Q}_{\mathcal{M}}(\tau)\}\rangle\rangle/2 \qquad (15)$$
$$\mathcal{I}S^{\mathcal{M}}_{IQ}(x,t;\tau) = -i\langle\langle[\hat{I}_{\mathcal{M}}(x,t),\hat{Q}_{\mathcal{M}}(\tau)]\rangle\rangle/2 \qquad (16)$$

are the real and imaginary parts of the current-charge correlator in the detectors $\mathcal{M} = \mathcal{A}$ or $\mathcal{B}$ representing pure detector response functions. On the other hand, $\mathcal{R}S^{\rm irr}_{QQ}(\tau_{\mathcal{A}},\tau_{\mathcal{B}}) = \langle\langle\{\hat{Q}(\tau_{\mathcal{A}}),\hat{Q}(\tau_{\mathcal{B}})\}\rangle\rangle/2$ and $\mathcal{I}S^{\rm irr}_{QQ}(\tau_{\mathcal{A}},\tau_{\mathcal{B}}) = -i\langle\langle[\hat{Q}(\tau_{\mathcal{A}}),\hat{Q}(\tau_{\mathcal{B}})]\rangle\rangle/2$ are the real (symmetrized) and imaginary (anti-symmetrized) part of the *irreducible* charge-charge correlator of the scattering region $\mathcal{D}$ which we are interested in. Again, for good, i.e., fast $t_{\rm tun} \ll t_{\rm sys}$, detectors, the system quantities $\mathcal{I}S^{\rm irr}_{QQ}$ and $\mathcal{R}S^{\rm irr}_{QQ}$ are slowly varying on the time scales of the detectors and the response functions effectively are given by the zero frequency response functions $\mathcal{I}S^{\mathcal{M}}_{IQ,\omega=0}$ and $\mathcal{R}S^{\mathcal{M}}_{IQ,\omega=0}$. For the QPC detector with a symmetric scattering potential, the real part of the zero frequency response vanishes[27,28], i.e., $\mathcal{R}S^{\mathcal{M}}_{IQ,\omega=0} = 0$, and we arrive at the simple relation[36]

$$\mathcal{R}S^{\rm irr}_{I_{\mathcal{A}}I_{\mathcal{B}}}(x_{\mathcal{A}},t_{\mathcal{A}};x_{\mathcal{B}},t_{\mathcal{B}})$$
$$\approx \frac{E^{\mathcal{A}}_{\rm C}E^{\mathcal{B}}_{\rm C}}{\hbar^2}\mathcal{I}S^{\mathcal{A}}_{IQ,\omega=0}\mathcal{I}S^{\mathcal{B}}_{IQ,\omega=0}\mathcal{R}S^{\rm irr}_{QQ}(\xi_A,\xi_B) \qquad (17)$$

with $\xi_{\mathcal{M}} = t_{\mathcal{M}} - |x_{\mathcal{M}}|/v_{\rm F}$ for $\mathcal{M} = \mathcal{A},\mathcal{B}$. Hence, for weak coupling and good (i.e., fast) detectors, the measureable quantity is the symmetrized *irreducible* correlator $\mathcal{R}S^{\rm irr}_{QQ}(\xi_{\mathcal{A}},\xi_{\mathcal{B}}) = \langle\langle\{\hat{Q}(\xi_{\mathcal{A}}),\hat{Q}(\xi_{\mathcal{B}})\}\rangle\rangle/2$ which depends only on the time-difference $\Delta\xi = \xi_{\mathcal{A}} - \xi_{\mathcal{B}}$. Analyzing the measurement with a single detector $\mathcal{M}$, we find that the relation between the current-current and charge-charge correlators is of the form[34,35]

$$\mathcal{R}S^{\rm irr}_{I_{\mathcal{M}}I_{\mathcal{M}}}(t_2,t_1) \approx \mathcal{R}S^{{\rm irr},0}_{I_{\mathcal{M}}I_{\mathcal{M}}}(t_2,t_1) + (E_{\rm C}\mathcal{I}S^{\mathcal{M}}_{IQ,\omega=0}/\hbar)^2\mathcal{R}S^{\rm irr}_{QQ}(t_2-t_1) \qquad (18)$$

with $\mathcal{R}S^{{\rm irr},0}_{I_{\mathcal{M}}I_{\mathcal{M}}}(t_2,t_1)$ describing the intrinsic current fluctuations of the detector current giving rise to a reduced signal-to-noise ratio.

Finally, the measurable *reducible* charge-charge correlator that can be compared to the projected charge correlator Eq. (9) is given by

$$\mathcal{R}S_{QQ}(t_2-t_1) = \langle\hat{Q}\rangle^2 + \mathcal{R}S^{\rm irr}_{QQ}(t_1-t_2) = \langle\{\hat{Q}(t_2),\hat{Q}(t_1)\}\rangle/2. \qquad (19)$$

As for strong coupling, spin can be taken into account by considering the full charge operator $\hat{Q} = \hat{Q}_\uparrow + \hat{Q}_\downarrow$ in Eq. (19) and accounting for the statistical independence of $\hat{Q}_\uparrow$ and $\hat{Q}_\downarrow$.

III. CHARGE-CHARGE CORRELATORS

A. Symmetrized charge-charge correlator

The measurable quantity at weak coupling is the symmetrized charge-charge correlator $\mathcal{R}S_{QQ}(t_2,t_1)$. Making use of Eq. (3) expressing the charge $\hat{Q}(t)$ in region $\mathcal{D}$ through the matrix $\mathbf{A}_{k',k}(t)$ and the density matrix $\hat{\rho}_0$ we obtain the result

$$\mathcal{R}S_{QQ}(t_2,t_1) = \Big(\sum_\alpha A_{\alpha,\alpha}n_\alpha\Big)^2 + \frac{1}{2}\sum_{\alpha,\beta}A_{\alpha,\beta}(t_2)A_{\beta,\alpha}(t_1)\big[n_\alpha(1-n_\beta)+n_\beta(1-n_\alpha)\big], \qquad (20)$$

with the occupation numbers $n_\alpha = n_{ak} = f(\epsilon_k - \mu_a)$. Below, we will compare this correlator to the projected charge-charge correlator $S^P_{QQ}(t_2,t_1)$.

B. Projected charge-charge correlator

Starting from the expression (9) for the projected charge-charge correlator, we make use of the Poisson formula $\sum_N e^{i(\lambda-\lambda')N} = \sum_M 2\pi\delta(\lambda-\lambda'+2\pi M)$ to rewrite the projected charge in the form

$$\hat{Q}^P(t_2|t_1) = \int_0^{2\pi}\frac{d\lambda}{2\pi}e^{-i\lambda\hat{Q}(t_1)}\hat{Q}(t_2)e^{i\lambda\hat{Q}(t_1)}. \qquad (21)$$

Using the projector property of $\mathbf{A}$, see Eq. (6), we find for the commutators (we adopt the notation in Eq. (4))

$$[e^{-i\lambda\hat{Q}(t_1)},\hat{c}^\dagger_{\alpha'}] = (e^{-i\lambda}-1)\sum_{\gamma'} A_{\alpha',\gamma'}(t_1)\hat{c}^\dagger_{\gamma'}e^{-i\lambda\hat{Q}(t_1)},$$
$$[\hat{c}_\alpha, e^{i\lambda\hat{Q}(t_1)}] = e^{i\lambda\hat{Q}(t_1)}(e^{i\lambda}-1)\sum_{\gamma}\hat{c}_\gamma A_{\gamma,\alpha}(t_1), \quad (22)$$

and carrying out the integration in (21) over λ, the projected charge operator can be written as

$$\hat{Q}^P(t_2|t_1) = \sum_{\alpha'\alpha} A^P_{\alpha',\alpha}(t_2|t_1)\hat{c}^\dagger_{\alpha'}\hat{c}_\alpha. \quad (23)$$

The matrix $\mathbf{A}^P_{k',k}$ associated with the projected charge assumes the form (in lead space)

$$\mathbf{A}^P_{k',k}(t_2|t_1) = \iint \frac{dp'}{2\pi}\frac{dp}{2\pi}\big[\mathbf{A}_{k',p'}(t_1)\mathbf{A}_{p',p}(t_2)\mathbf{A}_{p,k}(t_1) + \bar{\mathbf{A}}_{k',p'}(t_1)\mathbf{A}_{p',p}(t_2)\bar{\mathbf{A}}_{p,k}(t_1)\big] \quad (24)$$

with the matrix $\mathbf{A}_{k,p}(t)$ given by Eq. (5) and $\bar{\mathbf{A}}_{k,p}(t) \equiv 2\pi\delta(k-p)\mathbf{1} - \mathbf{A}_{k,p}(t)$. Finally, the projected reducible charge-charge correlator S^P_{QQ} can be expressed in the form

$$S^P_{QQ}(t_2,t_1) = \sum_\alpha A^P_{\alpha,\alpha}(t_2|t_1)n_\alpha \sum_\beta A_{\beta,\beta}(t_1)n_\beta + \frac{1}{2}\sum_{\alpha,\beta} A^P_{\alpha,\beta}(t_2|t_1)A_{\beta,\alpha}(t_1)\big[n_\alpha(1-n_\beta)+n_\beta(1-n_\alpha)\big], \quad (25)$$

where the first contribution corresponds to the product $\langle\hat{Q}^P(t_2|t_1)\rangle\langle\hat{Q}(t_1)\rangle$. The comparison with the symmetrized correlator $\mathcal{R}S_{QQ}(t_2,t_1)$ found in Eq. (20) reveals quite some similarities, with one of the matrices $\mathbf{A}_{k',k}$ to be replaced by its projected version $\mathbf{A}^P_{k',k}$. Further below, we will analyze this correlator and compare it to the symmetrized correlator $\mathcal{R}S_{QQ}(t_2,t_1)$.

Before doing so, we show that the projected charge matrix elements in Eq. (24) can be simplified considerably. To this end, we derive a generalized version of Eq. (6) which involves different times t and s,

$$\int\frac{dp}{2\pi}\mathbf{A}_{k,p}(t)\mathbf{A}_{p,q}(s) = \Theta(s-t)\int\frac{dp}{2\pi}\Pi_{k,p}(t)\mathbf{A}_{p,q}(s) + \Theta(t-s)\int\frac{dp}{2\pi}\mathbf{A}_{k,p}(t)\Pi_{p,q}(s), \quad (26)$$

with the matrix elements $\Pi_{k,p}(t) = -ie^{i(k-p)(v_{\rm F}t+d/2)}/(k-p-i\delta)$ and $\Theta(t)$ the Heaviside function. Combining Eqs. (24) and (26) we obtain the projected charge matrix

$$\mathbf{A}^P_{k',k}(t_2|t_1) = \iint\frac{dp'}{2\pi}\frac{dp}{2\pi}\big[\Pi_{k',p'}(t_1)\mathbf{A}_{p',p}(t_2)\Pi_{p,k}(t_1) + \bar{\Pi}_{k',p'}(t_1)\mathbf{A}_{p',p}(t_2)\bar{\Pi}_{p,k}(t_1)\big], \quad (27)$$

where $\bar{\Pi}_{k,p}(t) = 2\pi\delta(k-p) - \Pi_{k,p}(t)$. Note the considerable simplification of this expression as compared to the original formula (24), where the structure of the region $\mathcal{D}$ encoded in the matrix elements $\mathbf{A}_{k',k}$ through the scattering matrices $\mathbf{S}^\dagger_{k'}$ and $\mathbf{S}_k$ appeared three times, while now only one matrix $\mathbf{A}_{p',p}$ remains. The result Eqs. (23) with (27) for the projected charge operator is the main technical result of this paper.

The generalized projector property Eq. (26) is related to the projector property of the charge operator $\hat{Q} = \hat{\mathcal{P}}_\mathcal{D}$ restricted to the single-particle Hilbert space. Expressing the field operators in $\int dx\,\hat{\psi}^\dagger(x)\hat{\psi}(x) = 1$ (restricted to the single-particle Hilbert space) through the scattering states, we can express $\hat{\mathcal{P}}_\mathcal{D}$ through the projectors onto the incoming and outgoing parts of the scattering states,

$$\hat{\mathcal{P}}_\mathcal{D}(t) = 1 - \hat{\mathcal{P}}_{\rm in}(t) - \hat{\mathcal{P}}_{\rm out}(t), \quad (28)$$

where $\hat{\mathcal{P}}_\nu(t) = \int dx\,\psi^\dagger_\nu(x,t)\psi_\nu(x,t)$ with $\nu = $ in/out. Here, we have used that ${}_\mathcal{D}\langle\varphi_{ak}|\varphi_{bq}\rangle_{\rm in/out} = 0$ and have neglected the small overlaps ${}_{\rm in}\langle\varphi_{ak}|\varphi_{bq}\rangle_{\rm out} = \mathcal{O}(1/k_{\rm F})$. Multiplying Eq. (28) by $\hat{\mathcal{P}}_\mathcal{D}(s)$ with $s>t$, we obtain the relation

$$\hat{\mathcal{P}}_\mathcal{D}(s)\hat{\mathcal{P}}_\mathcal{D}(t) = \hat{\mathcal{P}}_\mathcal{D}(s)[1-\hat{\mathcal{P}}_{\rm in}(t)], \quad (29)$$

where we could drop the term $\hat{\mathcal{P}}_\mathcal{D}(s)\hat{\mathcal{P}}_{\rm out}(t)$ since the outcoming component of a scattered particle cannot contribute to the charge on the dot at a later time. Expressing $\hat{\mathcal{P}}_\mathcal{D}$ through the charge matrix $\mathbf{A}_{k,p}$, see Eq. (5), and using $1-\hat{\mathcal{P}}_{\rm in}(t) = \iint(dk/2\pi)(dp/2\pi)\Pi_{k,p}(t)\hat{c}^\dagger_k\hat{c}_p$ with matrix elements $\Pi_{k,p}$ given above, we straightforwardly arrive at Eq. (26). Choosing $s<t$, we multiply Eq. (28) by $\hat{\mathcal{P}}_\mathcal{D}(s)$ from the right.

The two correlators $\mathcal{R}S_{QQ}(t_2,t_1)$ and $S^P_{QQ}(t_2,t_1)$ are formally different, see Eqs. (20) and (25). This implies that in the two limiting measurements, a different charge dynamics is detected due to the different back-action of the measurement onto the system. To study the difference between these two correlators beyond a formal level, we focus on the specific example of a single level quantum dot (modeled by the single resonance level model[32]) and investigate the differences between $\mathcal{R}S_{QQ}(t_2,t_1)$ and $S^P_{QQ}(t_2,t_1)$ quantitatively. In the end, we will draw some conclusions from this analysis for the general situation.

C. Single resonance level model

We model a single-level quantum dot scatterer by a single resonance level with a wavevector $k_{\rm res}$ defining its energy $\epsilon_{\rm res} = \epsilon_{\rm F} + \hbar v_{\rm F}(k_{\rm res}-k_{\rm F})$, a width γ (in k-space), and a parameter $\eta\in[-1,1]$ describing the asymmetry in the coupling to the two leads[32]. The unprojected charge matrix elements in Eq. (5) assume the simple form

$$A_{a'k',ak}(t) = a^*_{a'}a_a\left[\phi^*_{k'}(t)\phi_k(t)\right] \quad (30)$$

with $a_{L/R} = \pm i\sqrt{1\mp\eta}$ and $\phi_k(t) = \sqrt{\gamma}/(\delta k + i\gamma)\times e^{-i\delta k\, v_{\rm F}t}$ where $\delta k = k - k_{\rm res}$. Alternatively, the

charge operator can be expressed as $\hat{Q} = \hat{d}^\dagger \hat{d}$ with $\hat{d} = \sum_a \int (dk/2\pi) a_a \phi_k \hat{c}_{ak}$, where the operator $\hat{d}^\dagger$ creates a charge on the resonance level. This model describes a single spin-degenerate dot level in the non-interacting case with the spin trivially accounted for as noted above; alternatively, the model applies to the case of a dot with strong Coulomb interaction where at most one electron is present on the dot. In the following, we restrict ourselves to the discussion of the equilibrium case at zero temperature, i.e., $\mu_L = \mu_R$ and $T = 0$ (more precisely, we require that $k_B T < \max[|\epsilon_{\rm res} - \epsilon_F|, \hbar v_F \gamma]$). Eq. (4) combined with Eq. (30) then provide us with the equilibrium (steady-state) charge

$$Q = \langle \hat{Q}(t) \rangle = \sum_\alpha A_{\alpha,\alpha} n_\alpha = \int_{-\infty}^{\delta\kappa_F} \frac{d(\delta\kappa)}{\pi} \frac{1}{\delta\kappa^2 + 1}, \quad (31)$$

which is the measured dot occupation both for a strong- and a weak system–detector coupling.

a. Projected charge. First, we determine the expectation value of the projected charge operator $\hat{Q}^P(t|0)$, see Eq. (23). The measurement of this quantity involves two charge projections at times $t = 0$ and later at $t > 0$, where the outcome of the first measurement is disregarded. For the single resonance level, the projected charge matrix element Eq. (27) is given by

$$A^P_{a'k',ak}(t_2|t_1) = a^*_{a'} a_a \left[\phi^{P*}_{k'}(t_2|t_1) \phi^P_k(t_2|t_1) + (\phi^*_{k'}(t_2) - \phi^{P*}_{k'}(t_2|t_1))(\phi_k(t_2) - \phi^P_k(t_2|t_1)) \right] \quad (32)$$

with the projected amplitude $\phi^P_k(t_2|t_1) = \phi_k(t_1) \times e^{-\gamma v_F (t_2 - t_1)}$. The expectation value of the projected charge operator then takes the form

$$\langle \hat{Q}^P(t|0) \rangle = \int_{-\infty}^{\delta\kappa_F} \frac{d(\delta\kappa)}{\pi} \Big(\frac{e^{-2\tau}}{\delta\kappa^2 + 1} + \frac{|e^{i\delta\kappa\tau} - e^{-\tau}|^2}{\delta\kappa^2 + 1} \Big), \quad (33)$$

where we have introduced the dimensionless time $\tau = v_F \gamma t$ and the relative wave-vector $\delta\kappa = (k - k_{\rm res})/\gamma$.

The time dependence of $\langle \hat{Q}^P(t|0) \rangle$ for different positions of the resonance with respect to the Fermi level is plotted in Fig. 3. The data is (particle-hole) symmetric with respect to the resonance's position relative to the Fermi level, with the average projected charges below the Fermi level ($\delta\kappa_F > 0$) and symmetrically above ($-\delta\kappa_F$) related via

$$\langle \hat{Q}^P(t|0) \rangle_{\delta\kappa_F} = 1 - \langle \hat{Q}^P(t|0) \rangle_{-\delta\kappa_F}. \quad (34)$$

This symmetry enforces the projected charge to be equal to the equilibrium value for the resonance aligned with the Fermi level, $\langle \hat{Q}^P(t|0) \rangle_{\delta\kappa_F = 0} = 1/2$ at $\delta\kappa_F = 0$, see Fig. 3(a). Away from the Fermi level, the average projected charge at time $t > 0$ is suppressed in magnitude with respect to its equilibrium value $\langle \hat{Q}^P(t = 0|0) \rangle = Q$ and returns back as $t \to \infty$ with a typical equilibration time $t_{\rm eq} \sim 1/\gamma v_F |\delta\kappa_F|$.

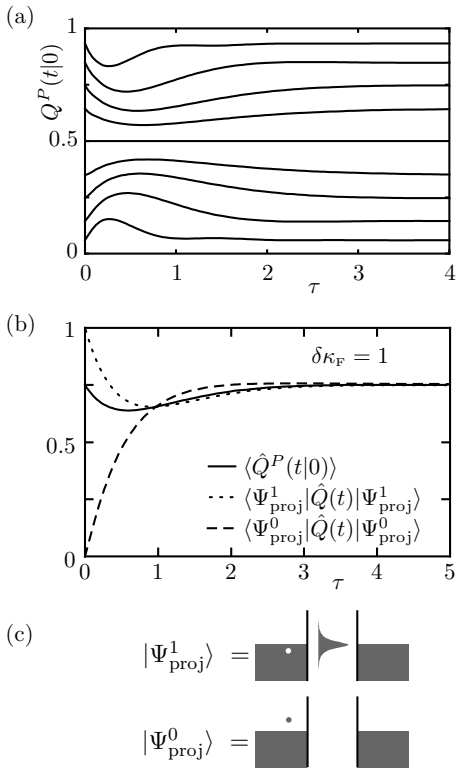

FIG. 3: (a) Charge expectation value $Q^P(t|0)$ for $\delta\kappa_F = \pm 5$, $\delta\kappa_F = \pm 2$, $\delta\kappa_F = \pm 1$, $\delta\kappa_F = \pm 0.5$, and $\delta\kappa_F = 0$. (b) Escape dynamics of the projected electron [hole] out of the dot described by $\langle \Psi^1_{\rm proj} | \hat{Q}(t) | \Psi^1_{\rm proj} \rangle$ (dotted) [$\langle \Psi^0_{\rm proj} | \hat{Q}(t) | \Psi^0_{\rm proj} \rangle$ (dashed)] resulting in the total projected charge dynamics $\langle \hat{Q}^P(t|0) \rangle$ (full line) for $\delta\kappa_F = 1$. (c) Sketch of two possible outcomes $|\Psi^1_{\rm proj}\rangle$ and $|\Psi^0_{\rm proj}\rangle$ of the charge projection at $t = 0$.

Consider, for example, a situation where the resonance is located below the Fermi level ($\delta\kappa_F > 0$). In this situation, it is more likely to observe an electron on the dot and thus one has $Q > 1/2$ in this regime. Surprisingly, the second projective measurement at $0 < t < t_{\rm eq}$ gives an average charge which is *smaller* than its equilibrium value (and correspondingly for $\delta\kappa_F < 0$). In order to understand the relaxation dynamics of $\langle \hat{Q}^P(t|0) \rangle$ it is instructive to analyze the evolution of the entire many-particle state right after the first projection. Consider again the situation where the resonance level is placed below the Fermi level. After the first projection, the dot is either occupied or empty, i.e., for zero temperature the state of the system is given by

$$|\Psi^N_{\rm proj}\rangle = \frac{\hat{P}_N |\Psi_{\rm eq}\rangle}{\sqrt{\langle \Psi_{\rm eq} | \hat{P}_N | \Psi_{\rm eq} \rangle}}, \quad N = 0,\ 1,$$

where the equilibrium state $|\Psi_{\rm eq}\rangle$ corresponds to a filled Fermi sea, see Fig. 3(c). Making use of the projectors $\hat{P}_0 = \hat{d}\hat{d}^\dagger$ and $\hat{P}_1 = \hat{d}^\dagger \hat{d}$ one can see, that for both measurement outcomes $N = 0,\ 1$ the projection creates a

single electron-hole pair in the system. The hole then screens the excess charge on the dot and gives rise to a Friedel-type oscillation of the charge distribution around the dot due to the sharp Fermi edge at zero temperature. Assume the first measurement results in an outcome $N = 1$ increasing the charge value on the dot above the equilibrium value. Since the projection is local, the accompanying hole is also created near the dot. During the subsequent evolution the charge in the dot can equilibrate in two ways: 1) the electron in the dot can tunnel out above the Fermi sea, or 2) it can tunnel out below the Fermi sea and fill the hole state. The appearance of the second relaxation channel enhances the electron escape rate that gives rise to the reduction of the average charge value below the equilibrium level, see Fig. 3(b). The same picture holds for the state $|\Psi^0_{\rm proj}\rangle$ with the excess hole in the dot compensated by an excess electron screening the charge outside the dot. Finally, the projected charge expectation value $\langle\hat{Q}^P(t|0)\rangle$ is a weighted average of the two processes corresponding to the two alternatives $N = 0,\ 1$ of the first projection, $\langle\hat{Q}^P(t|0)\rangle = \langle\hat{Q}\rangle\langle\Psi^1_{\rm proj}|\hat{Q}(t)|\Psi^1_{\rm proj}\rangle + (1-\langle\hat{Q}\rangle)\langle\Psi^0_{\rm proj}|\hat{Q}(t)|\Psi^0_{\rm proj}\rangle$, see Fig. 3(b).

The creation of the electron hole-pair due to the projection of the charge provides energy to the system. The average energy of the excited electron-hole pair is given by $\epsilon_{ph} = \sum_N\langle\hat{H}\hat{P}_N\rho_0\hat{P}_N\rangle - \langle\hat{H}\rho_0\rangle$,

$$\epsilon_{ph} = 2\int_{k_{\rm F}}^{\infty}\frac{dk}{\pi}\int_{-\infty}^{k_{\rm F}}\frac{dq}{\pi}\frac{(\epsilon_k-\epsilon_q)}{[\delta k^2+\gamma^2][\delta q^2+\gamma^2]}. \qquad (35)$$

This integral is divergent for the linear dispersion $\epsilon_k = \epsilon_{\rm F}+\hbar v_{\rm F}(k-k_{\rm F})$ [the same is true for the quadratic dispersion as well (with $q > 0$ in Eq. (35))], a consequence of the description of the projection as an instantaneous process. In an experimental realization the measurement involves a finite time and provides a finite amount of energy to the system, hence the particle-hole pair involves a finite energy. E.g., for the case of single-electron projection with a strong Coulomb coupling $E_{\rm C} > h\Gamma$ the measurement time is given by the tunneling time $t_{\rm tun} \sim 1/\Gamma$ and the energy exchange between the system and the detector is limited by $E_{\rm C}$; on the other hand, the measurement process should provide the energy for a 'reasonable' electron-hole pair (defining one electron or hole in the dot) given by $\epsilon_{ph} \sim |\epsilon_{\rm F} - \epsilon_{\rm res}|$. For a resonance overlapping with the Fermi level $|\epsilon_{\rm F}-\epsilon_{\rm res}| < hv_{\rm F}\gamma$ and a fast measurement with $t_{\rm tun} \ll t_{\rm sys} \sim 1/v_{\rm F}\gamma$ the Coulomb energy exceeds the electron-hole energy as $E_{\rm C} > h\Gamma \gg hv_{\rm F}\gamma \sim \epsilon_{ph}$. In the case of a multi-electron projection with $E_{\rm C} \ll h\Gamma$, each individual QPC electron provides a small amount of energy $\sim E_{\rm C}$ exciting the system to a virtual state and the overall process creates the resulting electron-hole pair in a similar way as the ionization via multi-photon absorption[41].

b. Charge-charge correlator. When discussing the charge-charge correlator, it is convenient to subtract the asymptotic value $\langle\hat{Q}\rangle^2 = Q^2$ and define $\Delta(\mathcal{R}S_{QQ}) = \mathcal{R}S_{QQ} - Q^2$ (which corresponds to the irreducible correlator) and $\Delta S^P_{QQ} = S^P_{QQ} - Q^2$. For a single resonance level, the correlator $\Delta(\mathcal{R}S_{QQ})$ as given by Eq. (20) takes the form

$$\Delta(\mathcal{R}S_{QQ})(t=\tau/\gamma v_{\rm F},0) \qquad (36)$$
$$= e^{-\tau}\int_{-\infty}^{\delta\kappa_{\rm F}}\frac{d(\delta\kappa)}{\pi}\frac{\cos(\delta\kappa\,\tau)}{\delta\kappa^2+1} - \Big|\int_{-\infty}^{\delta\kappa_{\rm F}}\frac{d(\delta\kappa)}{\pi}\frac{e^{i\delta\kappa\,\tau}}{\delta\kappa^2+1}\Big|^2.$$

On the other hand, the projected correlator ΔS^P_{QQ} follows from Eq. (25) and reads

$$\Delta S^P_{QQ}(t,0) = Qe^{-2\tau} - \Big|\int_{-\infty}^{\delta\kappa_{\rm F}}\frac{d(\delta\kappa)}{\pi}\frac{e^{i\delta\kappa\,\tau}}{\delta\kappa^2+1}\Big|^2 \qquad (37)$$

with the equilibrium charge expectation value Q given in Eq. (31). Due to particle-hole symmetry, both correlators Eqs. (36) and (37) remain unchanged when replacing $\delta\kappa_{\rm F} \to -\delta\kappa_{\rm F}$. Furthermore, the difference between the two correlators is given by the first terms and vanishes as $\delta\kappa_{\rm F} \to \pm\infty$ (filled and empty dot, unaltered by the projection) as well as at the particle-hole symmetric point at half-filling, $\delta\kappa_{\rm F} = 0$.

Analyzing the time dependence of the two correlators, see Figs. 4 (a)-(d), we observe that both correlators become negative at $t \sim 1/\gamma v_{\rm F}|\delta\kappa_{\rm F}|$ (cut off at $t \sim 1/\gamma v_{\rm F}$ as $|\delta\kappa_{\rm F}|$ drops below unity) indicating the anti-correlation in the system: detecting a particular charge value on the dot at $t = 0$, the observed charge state of the dot after the tunneling time is more likely to be inverse. At large times both correlators show a weak oscillating behavior approaching $\Delta\mathcal{R}S_{QQ}(t\to\infty,0) = \Delta S^P_{QQ}(t\to\infty,0) \to 0$ and the full charge-charge correlator assumes its asymptotic value Q^2. Comparing the two correlators with one another, we identify two regimes: (1) For $\delta\kappa_{\rm F} \lesssim 1$, the

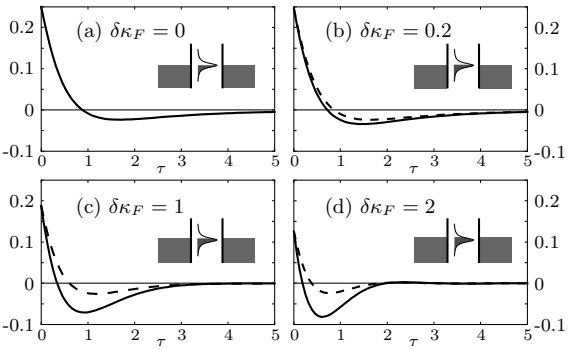

FIG. 4: The correlators $\Delta\mathcal{R}S_{QQ}(t,0)$ (dashed line) and $\Delta S^P_{QQ}(t,0)$ (full line) as a function of the dimensionless time $\tau = \gamma v_{\rm F}t$ for different values of the dimensionless resonance position $\delta\kappa_{\rm F} = (k_{\rm F} - k_{\rm res})/\gamma$. While the two correlators are similar for small $\delta\kappa_{\rm F}$ (see (a) $\delta\kappa_{\rm F} = 0$ and (b) $\delta\kappa_{\rm F} = 0.2$), for larger $\delta\kappa_{\rm F}$, the difference between the two correlators is more pronounced [(c) $\delta\kappa_{\rm F} = 1$ and (d) $\delta\kappa_{\rm F} = 2$]. The absolute value of the correlators decreases for increasing $\delta\kappa_{\rm F}$ such that in the limit $\delta\kappa_{\rm F} \to \infty$ both correlators vanish.

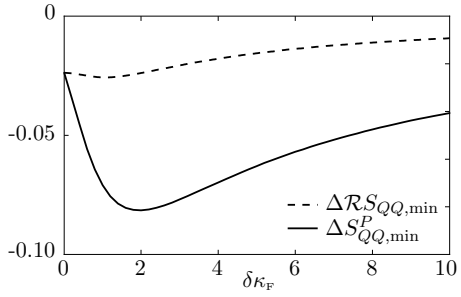

FIG. 5: The minima of $\Delta\mathcal{R}S_{QQ,\min} \equiv \min_t \mathcal{R}\Delta S^P_{QQ}(t,0)$ (dashed line) and $\Delta S^P_{QQ,\min} \equiv \min_t \Delta S_{QQ}(t,0)$ (full line) as a function of the dimensionless resonance position $\delta\kappa_F = (k_F - k_{res})/\gamma$. The anticorrelation dip is much more pronounced for the projected correlator.

system is close to the particle-hole symmetric point and the time-dependence of the two correlators is qualitatively the same with only a small quantitative difference. (2) When the Fermi level is away from the resonance level, the two correlators deviate considerably as the projection enhances the non-equilibrium behavior of the charge at later times. Indeed, the projected correlator shows a larger anti-correlation and more pronounced oscillations than the symmetric one, see Fig. 5.

The following general conclusions can be drawn from the above results: If the region $\mathcal{D}$ is in a well-defined charge state, the two correlators are identical as the projection due to the first charge measurement does not alter the state. For small deviations from a well-defined charge state, the difference between the two correlators remains small. The same is true for a system with particle-hole symmetry, as discussed for the half-filled dot above. If the system is in a superposition of different charge states with similar weights (but away from a particle-hole symmetric point), the projection has a pronounced impact on the measurement outcome and the two correlators $\mathcal{R}S_{QQ}(t,0)$ and $S^P_{QQ}(t,0)$ can deviate considerably with specific details depending on the scattering matrix of the system.

IV. EFFECT OF MULTIPLE PROJECTIVE MEASUREMENTS

So far, we have discussed two regimes of measuring the time-resolved charge-charge correlator: i) by projections (strong measurements) at times t_1 and t_2, or ii) by a weak measurement where the charge-charge correlator is obtained from a deconvolution of the detector current-current correlator and the detector response function. While in the latter case, the detector current may be applied continuously, for the strong measurement it is crucial to measure the charge at two times in a strong manner and allow for an unperturbed evolution in-between. Let us compare these two regimes to a typical experimental situation[24]: In these experiments, a fixed voltage V is applied at the detector which thus is constantly monitoring the charge of the system; at the same time, the clear steps visible in the detector-current traces indicate a strong measurement. Given the constant monitoring of the dot charge, the system is always perturbed. Furthermore, while our analysis above assumes a fully coherent evolution of the system, the coupling to the environment leads to a further decoherence beyond the one introduced by the measurement. Our model of a projective measurement of the charge-charge correlator $S^P_{QQ}(t_2,t_1)$ with an initial projection at time t_1 and a final projection at time t_2 is inappropriate to describe these measurements.

In the following, we formulate the continuous strong measurement discussed above and derive the appropriate charge-charge correlator. Following the general spirit of the paper, we model the continuous strong measurement by repeated projective measurements of the system. We introduce the formalism of multiple projective measurements and present the results for the multiple projected charge expectation value as well as the multiple projected charge-charge correlator. We identify a critical measurement rate where the dynamics of the charge changes from a system property to a regime where it is dominated by the measurement, becoming universal in the limit of a high projection rate. In the end, we discuss the rate at which we should project the system in order to model a realistic continuous measurement and compare to experiments.

A. Charge expectation value

Starting from the situation where we project the density matrix $\hat\rho_0$ once, see Sec. III B above, we account for n projections at times $t_1 < \ldots < t_n$ via the multiply projected density matrix

$$\sum_{N_1,\ldots,N_n} \mathcal{T}\Big[\prod_{i=1}^n \hat P_{N_i}(t_i)\Big]\hat\rho_0\tilde{\mathcal{T}}\Big[\prod_{i=1}^n \hat P_{N_i}(t_i)\Big] \qquad (38)$$

with the time-ordering operator $\mathcal{T}$ and the anti-time-ordering operator $\tilde{\mathcal{T}}$. The charge expectation at time $t > t_n$ after n previous projections at times $t_1 < \ldots < t_n$ is given by the expression

$$\begin{aligned}&\sum_{N_1,\ldots,N_n} \mathrm{Tr}\Big\{\hat Q(t)\mathcal{T}\Big[\prod_{i=1}^n \hat P_{N_i}(t_i)\Big]\hat\rho_0\tilde{\mathcal{T}}\Big[\prod_{i=1}^n \hat P_{N_i}(t_i)\Big]\Big\}\\ &= \sum_{N_1,\ldots,N_n} \mathrm{Tr}\Big\{\tilde{\mathcal{T}}\Big[\prod_{i=1}^n \hat P_{N_i}(t_i)\Big]\hat Q(t)\mathcal{T}\Big[\prod_{i=1}^n \hat P_{N_i}(t_i)\Big]\hat\rho_0\Big\}\\ &\equiv \langle\hat Q^{mP}(t|\{t_j\})\rangle, \qquad (39)\end{aligned}$$

where we have used again the trace property $\mathrm{Tr}(\hat A\hat B) = \mathrm{Tr}(\hat B\hat A)$ and we have introduced the multiply projected charge operator $\hat Q^{mP}(t|\{t_j\})$ with the projection times $\{t_j\} \equiv t_1,\ldots,t_n$. The latter can be

expressed as $\hat{Q}^{mP}(t|\{t_j\}) = \sum_{\alpha',\alpha} A^{mP}_{\alpha',\alpha}(t|\{t_j\})\hat{c}^\dagger_{\alpha'}\hat{c}_\alpha$ with matrix elements $A^{mP}_{\alpha',\alpha}(t|\{t_j\})$. To obtain these matrix elements, the projection operators can be taken into account iteratively, i.e., $\hat{Q}^{mP}(t|t_n,\ldots,t_i) = \sum_{N_i}\hat{P}_{N_i}(t_i)\hat{Q}^{mP}(t|t_n,\ldots,t_{i+1})\hat{P}_{N_i}(t_i)$. Making use of Eq. (26) and the property $\int(dq/2\pi)\Pi_{pq}(t)\Pi_{qk}(t') = \Pi_{pk}(t_{\rm min})$ with $t_{\rm min} = \min(t,t')$, the resulting matrix element can be simplified to

$$\hat{\mathbf{A}}^{mP}_{k',k}(t|\{t_j\}) = \iint \frac{dp'}{2\pi}\frac{dp}{2\pi}\Big[\Pi_{k'p'}(t_1)\mathbf{A}_{p',p}(t)\Pi_{pk}(t_1) + \sum_{i=1}^{n-1}\big[\Pi(t_{i+1})-\Pi(t_i)\big]_{k'p'}\mathbf{A}_{p',p}(t)\big[\Pi(t_{i+1})-\Pi(t_i)\big]_{pk} + \bar{\Pi}_{k'p'}(t_n)\mathbf{A}_{p',p}(t)\bar{\Pi}_{pk}(t_n)\Big]. \quad (40)$$

1. Single resonance level model

The relevant timescale in the description of (multiple) projections of the mean charge is the equilibration time $\tau_{\rm eq} = \gamma v_{\rm F} t_{\rm eq} \sim 1/\delta\kappa_{\rm F}$ (for $\delta\kappa_{\rm F} \gg 1$). For multiple projections, there are two regimes: if the time between subsequent projections $\delta t = \delta\tau/v_{\rm F}\gamma$ exceeds the equilibration time, $\delta t > t_{\rm eq}$, the projections are independent, see Fig. 6 (dashed line) for a plot of the corresponding multiply projected charge $Q^{mP,\delta t}(t) \equiv \langle\hat{Q}^{mP}(t|\{t_j = (j-1)\delta t\})\rangle$. On the other hand, for short intervalls $\delta t < t_{\rm eq}$, the system is not in equilibrium when the next projection occurs; multiple charge projections with small equal time steps δt then drive the system to a new steady state, see Fig. 6 (thin line).

When the Fermi energy resides above the resonance level ($\delta\kappa_{\rm F} > 0$), the new 'steady state' corresponds to a lower occupation of the dot state than in equilibrium, while for a resonance level above the Fermi energy ($\delta\kappa_{\rm F} < 0$), the dot occupation is increased. Frequent projection pushes the steady state occupation towards 1/2, see Fig. 6. For $|\delta\kappa_{\rm F}|\delta\tau \ll \pi$, the steady state occupation (at the times of projection) is given by

$$\lim_{\delta t\to 0} Q^{mP,\delta t}(t) = \frac{1}{2} + \frac{\delta\kappa_{\rm F}\delta\tau}{2\pi}, \quad (41)$$

i.e., the dot occupation is 1/2 up to a small correction. We can attribute this universal behavior (independent of applied chemical potentials) to an effective 'broadening' of the level over the width $h/\delta t$ in energy—as this width becomes much larger than the distance $\hbar v_{\rm F}|\delta k_{\rm F}|$ of the resonance level to the Fermi level, the dot is filled and emptied with equal probability.

2. Comparison to experiment

Let us compare these results and in particular the appearance of a universal regime with a charge expectation value 1/2 to the experiments by Gustavsson *et al.*[24]; as it turns out, this experiment is not dominated by the measurement but rather by temperature and no universal behavior is expected. The experimental setup consists of a QPC detector which is measuring the charge states $|N\rangle$ or $|N+1\rangle$ of a capacitively coupled quantum dot. The QPC detector is driven with a constant voltage $V_{\rm QPC} \sim 500\,\mu$V producing a current $I_{\rm in} \sim 20\,$nA which corresponds to electrons impinging on the QPC at a rate $1/t_{\rm V} \sim 10^{11}\,$Hz. From the current steps, we conclude that the transmissions corresponding to the two charge states are given by $T_{|N\rangle} \sim 0.3$ and $T_{|N+1\rangle} \sim 0.2$, implying a coupling $E_{\rm C}/h\Gamma \sim 0.1$. Making use of Eq. (11), we obtain that $N = t_{\rm ms}/t_V \sim 20$ electrons determine the dot state. For each data point, the QPC current is integrated during $t_{\rm dp} \sim 50\,\mu$s such that $6.\,10^6$ electrons pass through the QPC, which is far larger than $N_{\rm proj} \sim 20$. With $t_{\rm dp} < t_{\rm sys}$ every data point then provides the information of the actual charge state of the dot. The system lifetime derives from the step widths (of order $t_{\rm sys} \sim 1$ ms) of the measurement tracks and amounts to $h/t_{\rm sys} \sim 10^{-5}\,\mu$eV. We model the effect of the continuous measurement by repeated projections on the time scale $\delta t \sim t_{\rm ms}$, that provides an effective level broadening $h/t_{\rm ms} \sim 2\,\mu$eV. This value is far below the temperature scale[24] $k_{\rm B}T \sim 20\,\mu$eV (at $T \sim 230\,$mK). Alternatively, the system is drive-dominated when $V_{\rm QD} > k_{\rm B}T$, see Ref. 24.

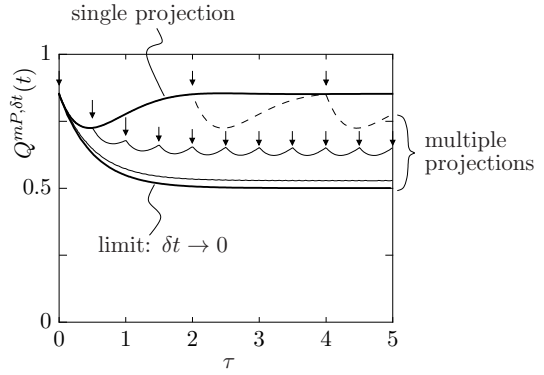

FIG. 6: For a single initial projection, the charge $Q^P(t|0)$ returns to the equilibrium value after a characteristic time scale $t_{\rm eq}$ (upper thick line, we choose $\delta\kappa_{\rm F} = (k_{\rm F}-k_{\rm res})/\gamma = 2$). For multiple projections (indicated by arrows) with time steps δt, we find two different behaviors for the charge $Q^{mP,\delta t}(t)$: For $\delta t > t_{\rm eq}$, the dot returns to the equilibrium before the next projection (dashed line, $\delta t = 2/\gamma v_{\rm F}$), while this is not the case when $\delta t < t_{\rm eq}$ and the system is driven to a new steady state (upper thin line, $\delta t = 1/2\gamma v_{\rm F}$). For faster projections (lower thin line, $\delta t = 1/10\gamma v_{\rm F}$), the occupation value is driven towards 1/2 (with the limit $\delta t \to 0$ indicated by the lower thick line).

B. Charge-charge correlator

Next, we investigate the effect of multiple projections on the charge-charge correlator. We consider the correlator between charges at times t_1 and t with multiple projections at times t_i in-between, assuming a free evolution of the system at times prior to the first measurement at t_1. The corresponding correlator is given by

$$\begin{aligned} &S^{mP}_{QQ}(t,t_1|\{t_j\}) \\ &= \sum_{N_1,\ldots,N_n} \mathrm{Tr}\Big\{\hat{Q}(t)\mathcal{T}\Big[\prod_{i=1}^{n}\hat{P}_{N_i}(t_i)\Big]\hat{Q}(t_1)\hat{\rho}_0\tilde{\mathcal{T}}\Big[\prod_{i=1}^{n}\hat{P}_{N_i}(t_i)\Big]\Big\} \\ &= \mathrm{Tr}\Big\{\hat{Q}^{mP}(t|\{t_j\})\hat{Q}(t_1)\hat{\rho}_0\Big\}, \end{aligned} \tag{42}$$

where we have used the trace property and the definition of the multiply projected charge operator $\hat{Q}^{mP}(t|\{t_j\})$. Making use of the matrix elements $A^{mP}_{\alpha,\beta}(t|\{t_j\})$ in Eq. (40), the charge-charge correlator can be expressed as

$$\begin{aligned} S^{mP}_{QQ}(t,t_1|\{t_j\}) =& \sum_{\alpha} A^{mP}_{\alpha,\alpha}(t|\{t_j\})n_\alpha \sum_{\beta} A_{\beta,\beta}(t_1)n_\beta \\ &+ \frac{1}{2}\sum_{\alpha,\beta} A^{mP}_{\alpha,\beta}(t|\{t_j\})A_{\beta,\alpha}(t_1)\big[n_\alpha(1-n_\beta)+n_\beta(1-n_\alpha)\big], \end{aligned} \tag{43}$$

where the first contribution is $\langle\hat{Q}^{mP}(t|\{t_j\})\rangle\langle\hat{Q}(t_1)\rangle$. Comparing this result to the case of a single projection discussed before, see Eq. (25), we recognize that the multiple projections enter through the matrix elements $A^{mP}_{\alpha,\beta}(t|\{t_j\})$ replacing the (singly projected) matrix element $A^{P}_{\alpha,\beta}(t|0)$.

1. Single resonance level model

For the single resonance level in equilibrium ($\mu_L = \mu_R = \epsilon_\mathrm{F}$) the charge matrix element assumes the simple form in Eq. (30). In Fig. 7 we compare the projected correlator $S^{P}_{QQ}(t,0)$ with the multiply projected correlator $S^{mP,\delta t}_{QQ}(t,0) \equiv S^{mP}_{QQ}(t,t_1=0|\{t_j=(j-1)\delta t\})$ with equal time separations $\delta t = \delta\tau/\gamma v_\mathrm{F}$ between projections; we consider the cases $\delta\tau = 1$ and $\delta\tau \to 0$. All correlators start out at $t=0$ with the value Q of the average charge Eq. (31). The correlator $S^{P}_{QQ}(t,0)$ then undergoes a pronounced anti-correlation dip and approaches $\langle\hat{Q}(t)\rangle\langle\hat{Q}(0)\rangle = Q^2$ for $t\to\infty$ (as the two charge states at 0 and t become uncorrelated). Repeated projections in between drive the correlator $S^{mP,\delta t}_{QQ}(t,0)$ towards $\langle\hat{Q}^{mP,\delta t}(t)\rangle\langle\hat{Q}(0)\rangle$ as the measurement induces an additional time dependence. In the limit of frequent projections, the projected charge expectation value $\langle\hat{Q}^{mP,\delta t}(t)\rangle$ approaches $1/2$ and hence the asymptotic value of the correlator is given by $S^{mP,\delta t\to 0}_{QQ}(t,0)\sim Q/2$. Overall, the result shows that only small times $\tau<1$ probe the system dynamics, while larger times become dominated by the measurement.

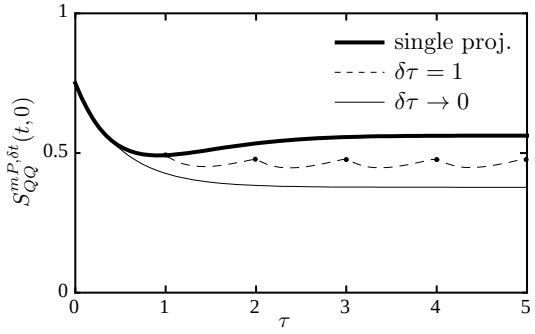

FIG. 7: $S^{mP,\delta t}_{QQ}(t,0)$ for multiple projections at $\delta\kappa_\mathrm{F}=1$: Single projected correlator (thick line), multiply projected correlator (dashed line, with $\delta\tau=1$ and dots indicating the projections), and the limiting behavior for $\delta t\to 0$ (thin line).

C. Fluctuating quantum dot level

We have seen that repeated projections with a time separation between subsequent projections approaching the Heisenberg time $h/|\epsilon_\mathrm{F}-\epsilon_\mathrm{res}|$ start dominating the dynamic evolution of the system and the average occupation number of the dot approaches the universal value $\langle\hat{Q}\rangle = 1/2$, irrespective of the position of the dot level with respect to the Fermi level, see Eq. (41). Here, we show how this formal result of the von Neumann projection postulate can be understood in terms of a measurement-induced fluctuation of the dot level. As before, we assume that the state of the dot is measured by a capacitively coupled QPC, see Fig. 8. We assume single electrons passing through the QPC with a frequency ν, e.g., due to an applied voltage V corresponding to $\nu = eV/h$, which corresponds to an incoming QPC current $I = e\nu$. An electron passing through the QPC interacts typically during a time $t_\mathrm{tun} = 1/\Gamma$ with the dot. The interaction strength is given by the Coulomb energy E_C. In our model, we take into account the effect of this current on the dot level ϵ_res via a classical electrostatic potential of the form $\epsilon_\mathrm{res}(t) = \epsilon_\mathrm{res} + \tilde{E}_\mathrm{C}\cos(2\pi\nu t)$ with an effective coupling strength $\tilde{E}_\mathrm{C} = E_\mathrm{C}\nu/\Gamma$ accounting for the typical interaction time $t_\mathrm{tun} = 1/\Gamma$. In order to describe the system, we define the time-dependent Hamiltonian

$$\begin{aligned} \hat{H}(t) =& \epsilon_\mathrm{res}(t)\hat{c}^\dagger\hat{c} + \int\frac{dk}{2\pi}\epsilon_k(\hat{a}^\dagger_k\hat{a}_k + \hat{b}^\dagger_k\hat{b}_k) \\ &+ \int\frac{dk}{2\pi}\big[\hbar v_\mathrm{F}\sqrt{\gamma_L}(\hat{a}^\dagger_k\hat{c}+h.c.) + \hbar v_\mathrm{F}\sqrt{\gamma_R}(\hat{b}^\dagger_k\hat{c}+h.c.)\big], \end{aligned} \tag{44}$$

where $\hat{a}_k$, $\hat{b}_k$ are the annihilation operators for the left and right reservoirs, $\hat{c}$ is the annihilation operator corresponding to the localized dot state, $\gamma_{L,R}$ are the partial widths of the level, $\epsilon_k = \epsilon_\mathrm{F} + \hbar v_\mathrm{F}(k-k_\mathrm{F})$ is the linearized dispersion of the lead electrons, and $\epsilon_\mathrm{res}(t)$ is the fluctuating energy of the dot. Solving the Heisenberg equation

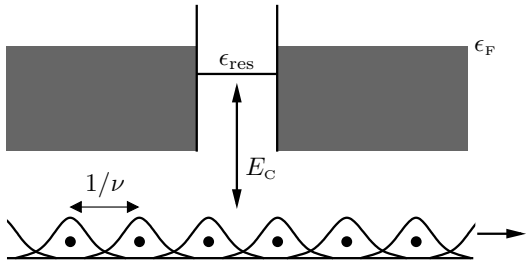

FIG. 8: A single resonance level at energy $\epsilon_{\rm res}$ coupled to two leads with states filled up to the Fermi energy $\epsilon_{\rm F}$ is capacitively interacting (with interaction strength $E_{\rm C}$) with the electrons passing through the QPC with frequency ν. We take this interaction into account via an effective time-dependent level energy $\epsilon_{\rm res}(t)$.

of motion, we obtain

$$\hat{c}(t) = \hat{c}(t_0)e^{-i\phi(t)+i\phi(t_0)-\gamma v_{\rm F}(t-t_0)/2} - iv_{\rm F}\int\frac{dk}{2\pi}(\sqrt{\gamma_L}\hat{a}_k+\sqrt{\gamma_R}\hat{b}_k) \times\int_{t_0}^{t}dt' e^{-i\phi(t)+i\phi(t')-\gamma v_{\rm F}(t-t')/2-i\epsilon_k(t'-t_0)/\hbar}, \tag{45}$$

where $\gamma=(\gamma_L+\gamma_R)$ is the resonance width and $\phi(t)=\int^t dt'\epsilon_{\rm res}(t')/\hbar$. Taking $t_0\to-\infty$ and $t=0$, the steady-state dot occupation is given by

$$\langle\hat{Q}\rangle=\langle\hat{c}^\dagger(0)\hat{c}(0)\rangle = v_{\rm F}^2\int\frac{dk}{2\pi}(\gamma_L n_{Lk}+\gamma_R n_{Rk}) \times\int_{-\infty}^{0}dt_1dt_2 e^{-i\phi(t_1)+i\phi(t_2)+\gamma v_{\rm F}(t_1+t_2)/2+i\epsilon_k(t_1-t_2)/\hbar}, \tag{46}$$

which in equilibrium, i.e., $n_{Lk}=n_{Rk}=\Theta(k_{\rm F}-k)$, simplifies to

$$\langle\hat{Q}\rangle=\gamma v_{\rm F}\int_{-\infty}^{0}\frac{dt_1dt_2}{2\pi i}\frac{e^{-i\phi(t_1)+i\phi(t_2)}}{t_1-t_2-i\delta}e^{\gamma v_{\rm F}(t_1+t_2)/2}e^{i\epsilon_{\rm F}(t_1-t_2)/\hbar}.$$

The phase $\phi(t)$ is of the form $\phi(t)=\epsilon_{\rm res}\,t/\hbar+(\tilde{E}_{\rm C}/h\nu)\sin(2\pi\nu t)$ and using the expansion $e^{iz\sin\theta}=\sum_n J_n(z)e^{in\theta}$, we can rewrite the expression above as

$$\langle\hat{Q}\rangle=\sum_{n,m=-\infty}^{\infty}J_n\Big(\frac{\tilde{E}_{\rm C}}{h\nu}\Big)J_m\Big(\frac{\tilde{E}_{\rm C}}{h\nu}\Big)\gamma v_{\rm F}\int_{-\infty}^{0}dt\,e^{\gamma v_{\rm F}t-i2\pi(n-m)\nu t} \times\int_{2t}^{-2t}\frac{d\tau}{2\pi i}\frac{e^{-i2\pi(n+m)\nu\tau+i(\epsilon_{\rm F}-\epsilon_{\rm res})\tau/\hbar}}{\tau-i\delta} \tag{47}$$

with $J_n(z)$ the Bessel functions of the first kind. Assuming frequent projections, $h\nu\gg|\epsilon_{\rm F}-\epsilon_{\rm res}|$, and a narrow resonance, $\hbar\gamma v_{\rm F}\ll|\epsilon_{\rm F}-\epsilon_{\rm res}|$, we can calculate $\langle\hat{Q}\rangle$ to leading order, where only terms $n=m\le 0$ contribute, and obtain

$$\langle\hat{Q}\rangle=\frac{1}{2}\Big[1+{\rm sgn}(\epsilon_{\rm F}-\epsilon_{\rm res})\,J_0^2\Big(\frac{\tilde{E}_{\rm C}}{h\nu}\Big)\Big], \tag{48}$$

where the identity $1=[J_0(x)]^2+2\sum_{\nu=1}^{\infty}[J_\nu(x)]^2$ has been used. Making use of $\tilde{E}_{\rm C}/h\nu=E_{\rm C}/h\Gamma$, we notice that for $E_{\rm C}>h\Gamma$, the steady-state charge $\langle\hat{Q}\rangle$ approaches the asymptotic value $1/2$. Hence, assuming a strong system-detector coupling with each electron realizing a strong projective measurement, we reproduce the case of frequent projective measurements discussed before, see Eq. (41). In order to reproduce the case of a projection by N electrons within a time $t_{\rm ms}$, we consider a periodic oscillation $\epsilon_{\rm res}(t)=\epsilon_{\rm res}+\tilde{E}_{\rm C}\cos(2\pi\tilde{\nu}t)$ of the dot level with frequency $\tilde{\nu}=\nu/N=1/t_{\rm ms}$ and effective Coulomb strength $\tilde{E}_{\rm C}=NE_{\rm C}\tilde{\nu}/\Gamma=E_{\rm C}\nu/\Gamma$. While this periodicity is artificially introduced here, it could be realized by switching the QPC current on and off repeatedly with this period. Adapting the calculation above, we obtain in the limit of fast projection $h\tilde{\nu}\gg|\epsilon_{\rm F}-\epsilon_{\rm res}|$ an average charge $\langle\hat{Q}\rangle=(1/2)[1+{\rm sgn}(\epsilon_{\rm F}-\epsilon_{\rm res})\,J_0^2(NE_{\rm C}/h\Gamma)]$, such that for $NE_{\rm C}>h\Gamma$ the system is driven to the universal regime as in the case of single electron projection discussed above. Within this treatment, it is the randomization of the dot level which leads to equal probabilities to find the level either empty or filled and which is responsible for the universal filling factor $1/2$.

V. CONCLUSION

We have studied the charge and charge-charge correlator of a quantum dot $\mathcal{D}$ (a localized region $\mathcal{D}$ of an arbitrary mesoscopic scatterer in more general terms). Making use of the single-particle scattering matrix of the scatterer $\mathbf{S}_k$, we expressed the charge operator $\hat{Q}(t)$ for $\mathcal{D}$ through the single-particle scattering matrix. In order to measure this charge, the system has been coupled to a detector; the measurement then acts back on the dot's occupation and therefore the charge dynamics depends on the coupling to the detector. We have focussed on a QPC detector which is capacitively coupled to the charge in region $\mathcal{D}$. We have analyzed different measurement regimes and identified two particular cases: at strong dot–detector coupling $E_{\rm C}>h\Gamma$, one single electron already can perform a strong measurement and project the system; such a strong/projective measurement is still possible even at intermediate coupling $E_{\rm C}<h\Gamma$ where many electrons accumulated over a measurement time $t_{\rm ms}$ are needed to project the dot-state, provided that $t_{\rm ms}$ remains below the system time $t_{\rm sys}$ where the charge on the dot changes. In our phenomenological approach, we have described such strong measurements with the help of the von Neumann projection postulate (maximal back action) and the measured charge-charge correlator is the projected quantity $S^P_{QQ}(t,0)$ involving the

projected charge operator $\hat{Q}^P(t|0)$. When the coupling is weak, $E_C \ll h\Gamma$ and $t_{ms} > t_{sys}$ the measurement is in the weak regime. We have analyzed this case in lowest-order perturbation theory (with vanishing back action) and have identified the symmetrized irreducible correlator $\mathcal{R}S_{QQ}(t,0)$ as the measurable quantity.

The difference between the strong and weak measurement regimes consists in the different degree the system becomes entangled with the detector during the systems's dynamical time. In a strong measurement, the projection of the detector degree of freedom implies a projection of the system's state, allowing to exclude the detector from the consideration. For the weak measurement, the system becomes only weakly entangled with the detector and almost preserves its coherent evolution; the detector's projection (involving a quasi-classical variable[37]) then acts only as a weak perturbation on the system's dynamics. Although the results for strong and weak measurements look quite different on a formal level, we find a qualitative correspondence when analyzing the expressions for a single-level quantum dot.

The projected charge correlator involves the projected charge operator $\hat{Q}^P(t|0)$ providing the charge at time t after a projection at an earlier time $t = 0$, see Eq. (23). A simple expression for this quantity (that could also be carried over to the case of multiply repeated projections) was obtained by making use of the analytic structure of the scattering matrix $\mathbf{S}_k$. The evolution of this projected charge, in particular, its initial decay in modulus and subsequent return to the equilibrium value, could be understood in terms of the generation of a particle-hole excitation in the nearby leads through the projection. In the limit of frequent projections, we have identified a transition from a regime where the dot dynamics is determined by the characteristics of the system to a regime where it is uniquely determined by the detector with universal outcome. In order to reproduce these results within a unitary treatment, we have modeled the projective measurements by a strongly fluctuating dot level.

The back-action of a measurement naturally manifests itself in the time-correlator of the measured quantity, as the second measurement probes both the dynamics of the system as well as the back-action on the system originating from the first measurement. Furthermore, the strength of the back-action increases from zero in a weak measurement to a maximum in a strong measurement described by the von Neumann projection scheme. Our analysis of time-correlators then provides insights on the range of back-action effects in a simple model setup.

We thank Simon Gustavsson and Oded Zilberberg for illuminating discussions and acknowledge financial support from the Swiss National Science Foundation through the National Center of Competence in Research on Quantum Science and Technology (QSIT), the Pauli Center for Theoretical Studies at ETH Zurich, and the RFBR Grant No. 14-02-01287.

[1] V.B. Braginsky and F.Y. Khalili, *Quantum Measurement* (Cambridge University Press, Cambridge, 1992).
[2] H.M. Wiseman and G.J. Milburn, *Quantum measurement and control* (Cambridge University Press, Cambridge, 2010).
[3] A.A. Clerk, M.H. Devoret, S.M. Girvin, F. Marquardt, and R.J. Schoelkopf, Rev. Mod. Phys. **82**, 1155 (2010).
[4] M. Born, Z. Phys. **37**, 863 (1926).
[5] J. von Neumann, *Mathematische Grundlagen der Quantentheorie* (Springer, Berlin, 1931).
[6] H. Everett, Rev. Mod. Phys. **29**, 454 (1957).
[7] R.B. Griffiths, *Consistent Quantum Theory* (Cambridge University Press, Cambridge, 2001).
[8] J.A. Wheeler and W.H. Zurek (eds.), *Quantum Theory and Measurement* (Princeton University Press, Princeton, 1983).
[9] W.H. Zurek, Rev. Mod. Phys. **75**, 715 (2003).
[10] D.V. Averin and E.V. Sukhorukov, Phys. Rev. Lett. **95**, 126803 (2005).
[11] I.L. Aleiner, N.S. Wingreen, and Y. Meir, Phys. Rev. Lett. **79**, 3740 (1997).
[12] Y. Levinson, Europhys. Lett. **39**, 299 (1997).
[13] A. Shnirman and G. Schön, Phys. Rev. B **57**, 15400 (1998).
[14] Y. Makhlin, G. Schön, and A. Shnirman, Phys. Rev. Lett. **85**, 4578 (2000).
[15] S.A. Gurvitz, Phys. Rev. B **56**, 15215 (1997).
[16] L. Stodolsky, Phys. Lett. B **459**, 193 (1999).
[17] A.N. Korotkov, Phys. Rev. B **60**, 5737 (1999).
[18] A.N. Korotkov, Phys. Rev. B **63**, 115403 (2001).
[19] Y. Aharonov, D.Z. Albert, and L. Vaidman, Phys. Rev. Lett. **60**, 1351 (1988).
[20] J. Dressel, M. Malik, F.M. Miatto, A.N. Jordan, and R.W. Boyd, Rev. Mod. Phys. **86**, 307 (2014).
[21] A. Romito, Y. Gefen, and Y.M. Blanter, Phys. Rev. Lett. **100**, 056801 (2008).
[22] O. Zilberberg, A. Carmi, and A. Romito, arXiv:1403.5897 (2014).
[23] E. Buks, R. Schuster, M. Heiblum, D. Malahu, and V. Umansky, Nature (London) **391**, 871 (1998).
[24] S. Gustavsson, R. Leturcq, B. Simovič, R. Schleser, T. Ihn, P. Studerus, K. Ensslin, D.C. Driscoll, and A.C. Gossard, Phys. Rev. Lett. **96**, 076605 (2006); S. Gustavsson, R. Leturcq, B. Simovič, R. Schleser, P. Studerus, T. Ihn, K. Ensslin, D.C. Driscoll, and A.C. Gossard, Phys. Rev. B **74**, 195305 (2006).
[25] M. Field, C.G. Smith, M. Pepper, D.A. Ritchie, J.E.F. Frost, G.A.C. Jones, and D.G. Hasko, Phys. Rev. Lett. **70**, 1311 (1993).
[26] L.M.K. Vandersypen, J.M. Elzerman, R.N. Schouten, L.H. Willems van Beveren, R. Hanson, and L.P. Kouwenhoven, Appl. Phys. Lett. **85**, 4394 (2004).
[27] A.A. Clerk, S.M. Girvin, and A.D. Stone, Phys. Rev. B **67**, 165324 (2003).
[28] S. Pilgram and M. Büttiker, Phys. Rev. Lett. **89**, 200401 (2002).
[29] G. Feve, A. Mahe, J.-M. Berroir, T. Kontos, B. Placais,

D.C. Glattli, A. Cavanna, B. Etienne, and Y. Jin, Science **316**, 1169 (2007).
[30] J. Dubois, T. Jullien, F. Portier, P. Roche, A. Cavanna, Y. Jin, W. Wegscheider, P. Roulleau, and D.C. Glattli, Nature **502**, 659 (2013).
[31] G.B. Lesovik and I.A. Sadovskyy, Phys. Usp. **54**, 1007 (2011).
[32] D. Oehri, A.V. Lebedev, G.B. Lesovik, and G. Blatter, Phys. Rev. B **86**, 125301 (2012).
[33] M.H. Pedersen, S.A. van Langen, and M. Büttiker, Phys. Rev. B **57**, 1838 (1998).
[34] A.N. Korotkov and D.V. Averin, Phys. Rev. B **64**, 165310 (2001).
[35] D.V. Averin, in *Exploring the Quantum-Classical Frontier: Recent Advances in Macroscopic and Mesoscopic Quantum Phenomena*, edited by J.R. Friedman and S. Han (Nova Science Publishers, New York, 2003), pp. 447-470.
[36] A.N. Jordan and M. Büttiker, Phys. Rev. Lett. **95**, 220401 (2005).
[37] G.B. Lesovik, Phys.-Usp. **41**, 145 (1998).
[38] G.B. Lesovik and R. Loosen, JETP Lett. **65**, 295 (1997).
[39] U. Gavish, Y. Levinson, and Y. Imry, Phys. Rev. B **62**, R10637 (2000).
[40] R. Aguado and L.P. Kouwenhoven, Phys. Rev. Lett. **84**, 1986 (2000).
[41] L.V. Keldysh, Sov. Phys. JETP **20**, 1307 (1965).